

Near-Global Variability of Stratospheric Water Vapor Observed by SAGE III/ISS

Key Points:

- Geophysical variability of the H₂O from the Stratospheric Aerosol and Gas Experiment III on the International Space Station (SAGE III/ISS) are evaluated
- Seasonal and interannual variations in stratospheric water vapor are consistent between SAGE III/ISS and Microwave Limb Sounder
- Large-scale variations in relative humidity highlight temperature control of water vapor near the tropopause






Correspondence to:

M. Park,
mijeong@ucar.edu

Citation:

Park, M., Randel, W. J., Damadeo, R. P., Flittner, D. E., Davis, S. M., Rosenlof, K. H., et al. (2021). Near-global variability of stratospheric water vapor observed by SAGE III/ISS. *Journal of Geophysical Research: Atmospheres*, 126, e2020JD034274. <https://doi.org/10.1029/2020JD034274>

Received 18 NOV 2020
 Accepted 16 MAR 2021

Mijeong Park¹ , William J. Randel¹ , Robert P. Damadeo², David E. Flittner², Sean M. Davis³ , Karen H. Rosenlof³ , Nathaniel Livesey⁴ , Alyn Lambert⁴, and William Read⁴

¹National Center for Atmospheric Research (NCAR), Atmospheric Chemistry Observations and Modeling (ACOM), Boulder, CO, USA, ²National Aeronautics and Space Administration (NASA), Langley Research Center, Hampton, VA, USA, ³National Oceanic and Atmospheric Administration (NOAA), Chemical Sciences Laboratory, Boulder, CO, USA, ⁴Jet Propulsion Laboratory (JPL), California Institute of Technology, Pasadena, CA, USA

Abstract The Stratospheric Aerosol and Gas Experiment III instrument on the International Space Station (SAGE III/ISS) has been making high quality solar occultation measurements of stratospheric water vapor since June 2017. Here we evaluate the large-scale geophysical variability of the SAGE III/ISS water vapor measurements for the first 3 years of observations (2017–2020) as part of data validation for retrieval version 5.1 (v5.1). Detailed comparisons of SAGE III/ISS v5.1 with the Aura Microwave Limb Sounder (MLS) version 5 retrievals show overall excellent agreement in terms of seasonal mean structure and large-scale variability. SAGE III/ISS data capture the well-known seasonal variations in water vapor including the vertically propagating “tape recorder” in the tropics and lower stratospheric maxima linked to the NH summer monsoons. The high vertical resolution (~2 km) measurements from SAGE III/ISS demonstrate contributions of the monsoons to the wet phase of “tape recorder” during the Northern Hemisphere (NH) summer. Interannual variations over the short data record are also consistent between SAGE III/ISS and MLS in the stratosphere between 16 and 30 km. We furthermore evaluate large-scale variations in relative humidity (RH) derived from the high vertical resolution SAGE III/ISS water vapor measurements, highlighting the detailed seasonal behavior and links to thermal structure near the tropical tropopause. Spatial distributions of RH at the cold point tropopause (CPT) show a close link between high RH and the minimum CPT temperature in both the NH winter and summer, consistent with temperature control of water vapor near the tropopause.

1. Introduction

Stratospheric water vapor is important for radiative and chemical influences on the climate system (e.g., Anderson et al., 2012; Forster & Shine, 2002) and continues to be a topic of interest for observations and model simulations (e.g., Avery et al., 2017; Banerjee et al., 2019; Dessler et al., 2013; Jensen et al., 2020; Schoeberl et al., 2019; Yue et al., 2019). Long-term observations of stratospheric water vapor are available from balloon measurements (Hurst et al., 2016), together with near-global measurements from satellite data. Satellite instruments with long-term satellite data records include measurements from the Stratospheric Aerosol and Gas Experiment II (SAGE II, 1984–2005; Damadeo et al., 2013; Thomason et al., 2004), the Halogen Occultation Experiment (HALOE, 1991–2005; Russell et al., 1993), the SAGE III instrument onboard the METEOR-3M satellite (SAGE III/M3M, 2002–2005; Thomason et al., 2010), the Aura Microwave Limb Sounder (MLS, 2004–present; Livesey et al., 2020; Waters et al., 2006), and the Atmospheric Chemistry Experiment Fourier Transform Spectrometer (ACE-FTS, 2004–present; Bernath et al., 2005) on board the SCISAT satellite (Boone et al., 2020). Long term observations of water vapor (H₂O) in the stratosphere and mesosphere have also been provided by the Sounding of the Atmosphere using Broadband Emission Radiometry (SABER, 2002–present; Rong et al., 2019) instrument. Davis et al. (2016) discusses data quality for the SAGE II, HALOE and MLS instruments, in addition to providing a homogenized, merged data set. A comprehensive overview of stratospheric water vapor measurements from satellites is presented in the second Stratosphere-troposphere Processes and their Role in Climate (SPARC) water vapor assessment (WAVASII; Lossow et al., 2017).

More recently, the Stratospheric Aerosol and Gas Experiment III on the International Space Station (SAGE III/ISS; Cisewski et al., 2014) has been making near-global measurements of stratospheric water vapor since June 2017. The objective of this study is to evaluate large-scale geophysical variability in SAGE III/ISS H₂O data as one component of data validation. This study is a companion to Davis et al. (2021), which focuses on detailed profile comparisons of SAGE III/ISS with correlative independent data sets and providing guidance for filtering data. Our analysis involves evaluating large-scale seasonal and interannual variability in SAGE III/ISS over 2017–2020, including detailed comparisons with MLS water vapor retrievals. The comparisons with the MLS data are valuable because of the very different spatiotemporal sampling of SAGE III/ISS and MLS. The solar occultation technique from SAGE III/ISS provides high vertical resolution measurements with limited spatial sampling (~31 solar occultation measurements per day), while passive limb sounding from MLS provides daily near-global observations (82°S–82°N) with lower vertical resolution. Note that the sampling differences can have a substantial impact on the depiction of stratospheric dynamics and trends as shown in Millán et al. (2016). Here, we focus on the large-scale seasonal and interannual variabilities with qualitative analyses. Our analyses of SAGE III/ISS data are based on recommended aerosol/cloud filtering parameters from Davis et al. (2021), but we also highlight sensitivity of these data to enhanced stratospheric aerosol loadings from volcanic eruptions (Chouza et al., 2020; Kloss et al., 2021) and stratospheric pyro-cumulonimbus (pyroCb) events (Fromm et al., 2010; Kablick et al., 2020; Khaykin et al., 2020). We also evaluate climatological upper troposphere-lower stratosphere (UTLS) relative humidity (RH) variations derived from SAGE III/ISS water vapor and co-located temperature and quantify their detailed relationships with UTLS thermal structure. The overall goal is to assess SAGE III/ISS H₂O data quality by evaluating large-scale geophysical variability in light of well-known behavior in the stratosphere, allowing use of these data to improve understanding of processes influencing stratospheric water vapor.

2. Data Description

2.1. SAGE III/ISS

The SAGE III, the second instrument from the SAGE III project (Chu & Veiga, 1998), was launched to the ISS on February 19, 2017 and began routine operations in June 2017. In a mid-inclination orbit of 51.6°, SAGE III/ISS (Cisewski et al., 2014; Lorelei et al., 1999) provides measurements of aerosol, ozone, water vapor, and other trace gases between 70°S and 70°N latitude using the techniques of solar occultation, lunar occultation, and limb scattering. Vertical profiles of water vapor are currently only produced from solar occultation data, which provide ~31 profiles per day. This study uses version 5.1 (v5.1) H₂O profiles, provided on a 0.5 km grid from 0.5–60.0 km, from June 2017 to May 2020. SAGE III/ISS water vapor retrieval is performed on a 1 km grid and the results are interpolated to a 0.5 km grid. These profiles are smoothed with a 1-2-1 filter in altitude, giving a vertical resolution of the v5.1 water vapor of ~2 km (see Davis et al., 2021 for details of the retrieval algorithm). Davis et al. (2021) also makes recommendations on filtering the data for retrieval anomalies and cloud interference that are applied here. The data are provided in units of number density on altitude and are converted to mixing ratio using the temperature and pressure profiles reported in the SAGE III/ISS data files that originate from the Modern-Era Retrospective analysis for Research and Applications, Version 2 (MERRA-2, Gelaro et al., 2017). Wang et al. (2020) discussed a small altitude registration error of ~100 m in the SAGE III/ISS v5.1 auxiliary temperature and pressure profiles reported in the data file. The temperature and pressure profiles used for the relative humidity calculations in this study are remapped after this altitude registration error is corrected. Note the SAGE III/ISS retrieval algorithm solves for H₂O mixing ratio and then converts to number density using the meteorological profiles reported in the file. This altitude registration error correction only applies to our relative humidity calculations and is not used for converting from number density to mixing ratio.

2.2. Aura MLS

The Earth Observing System (EOS) Microwave Limb Sounder (MLS) on board the Aura satellite was launched into a sun-synchronous near-circular polar orbit in July 2004 (Waters et al., 2006). The MLS instrument measures ~3,500 profiles per day between 82°S and 82°N latitude. We use the Level 2 (L2) MLS H₂O based on version 5 (v5.0) data (Lambert et al., 2020; Livesey et al., 2020). Note that this is a recent update from the MLS version 4.2 (v4.2) data used in Davis et al. (2021). Hurst et al. (2016) have shown that

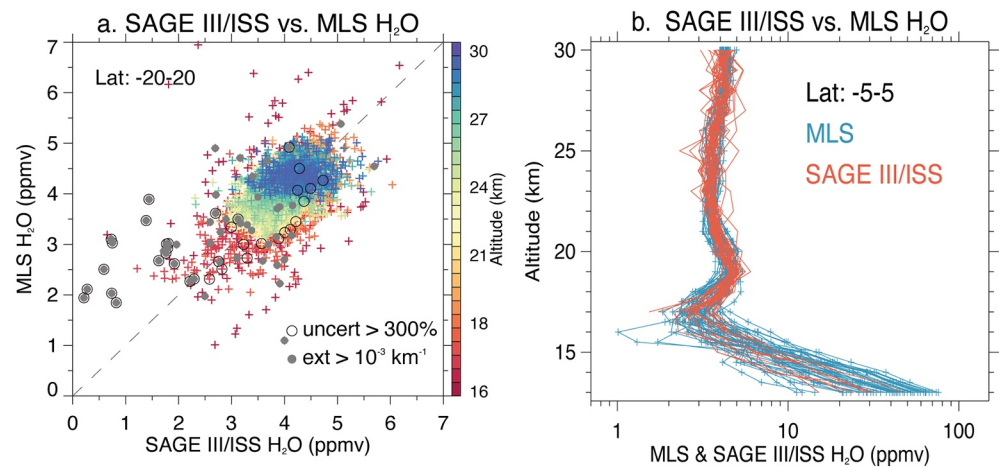


Figure 1. (a) Scatter plots of co-located SAGE III/ISS versus MLS water vapor (unit: ppmv) between 20°S and 20°N colored by altitude (16–30 km) in November 2017 before the filtering is applied. SAGE III/ISS water vapor profiles with high uncertainty (>300%) are marked as open circles and with aerosol extinction coefficient at 1,022 nm higher than $1 \times 10^{-3} \text{ km}^{-1}$ are marked as filled circles. (b) Vertical profiles of SAGE III/ISS (orange) and MLS v5.0 (blue) water vapor between 5°S and 5°N latitude for the same month. MLS, Microwave Limb Sounder; SAGE III/ISS, Stratospheric Aerosol and Gas Experiment III on the International Space Station.

the MLS v4.2 H₂O retrievals (Lambert et al., 2015) have temporal drift issues since ~2010, possibly related to aging of the instrument. MLS v5.0 corrects for the temporal calibration drift and also for a dry bias (~20%) below the tropopause. The changes made to v5.0 result in a ~5%–10% reduction in water vapor mixing ratios in the stratosphere and above compared to the previous versions. MLS H₂O profiles are reported on pressure grids (12 levels per decade, 316–0.001 hPa). For comparison with SAGE III/ISS, each MLS H₂O L2 profile is interpolated to an oversampled altitude grid (0.5 km interval) using the temperature and pressure profiles from MERRA-2. The MERRA-2 meteorological profiles are obtained from the Derived Meteorological Products (DMPs, see Manney et al., 2007; 2011). MLS daily average data are constructed on a 7.5° latitude × 15° longitude grid each day using the L2 data after applying data screening criteria (Livesey et al., 2020). MLS monthly average data are constructed by averaging daily data each month. For direct comparisons between MLS and SAGE III/ISS in Section 3.1, MLS data are interpolated to the SAGE III/ISS measurement locations, altitudes and time, as described in Davis et al. (2021).

3. Results

3.1. Comparisons With MLS and Filtering Cloud/Aerosol Influences in SAGE III/ISS Data

In this section, we show profile-to-profile comparisons between SAGE III/ISS and MLS H₂O and discuss details of the SAGE III/ISS data quality and screening. Davis et al. (2021) include extensive SAGE III/ISS comparisons with MLS v4.2 retrievals, showing an overall dry bias for SAGE III/ISS of ~10% in the stratosphere for June 2017–December 2019. Here we compare with the updated MLS v5.0 data, which is ~5%–10% drier than v4.2 in the stratosphere.

As an example, we show comparisons of MLS and SAGE III/ISS H₂O profiles in the tropics for November 2017. Figure 1a shows pointwise comparisons of SAGE III/ISS and MLS data over 16–30 km during November 2017 using all profiles between 20°N and 20°S, illustrating strong correlation with small biases, but with substantial scatter and numerous outliers, especially at low altitudes. Many of these outliers are associated with aerosol and cloud effects on retrievals. Both the water vapor signal and the inversion process are affected by the presence of clouds, as discussed in Davis et al. (2021). For instance, uncertainties in water vapor grow rapidly where the aerosol extinction at 1,022 nm exceeds $1 \times 10^{-3} \text{ km}^{-1}$. Davis et al. (2021) explains details on filtering anomalous events (i.e., unphysical negative outliers and so-called keel-over profiles at altitudes > 30 km) and developed a filtering method using a combination of aerosol extinction and color ratio as a conservative cloud filter. We have applied both retrieval uncertainty and aerosol extinction coefficient

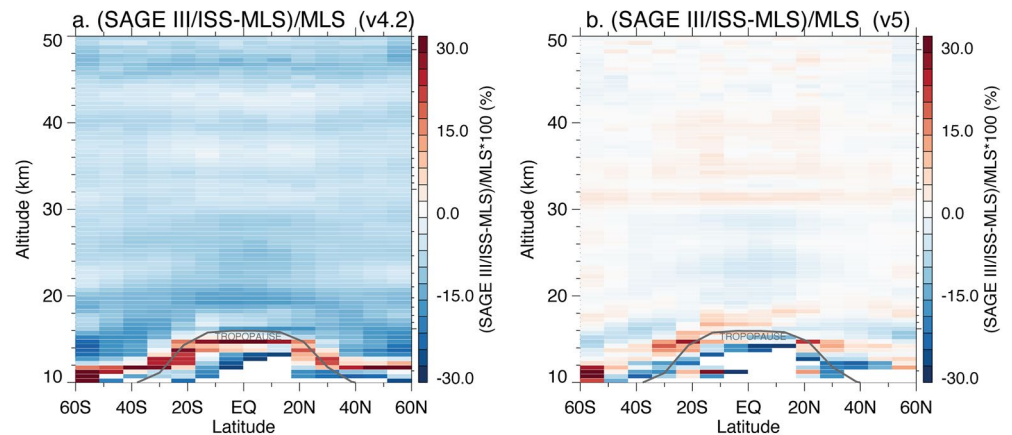


Figure 2. Relative difference between SAGE III/ISS and MLS water vapor medians ($[\text{SAGE III/ISS-MLS}]/\text{MLS} \times 100$, unit: %) calculated for June 2017–November 2020 for (a) MLS v4.2 and (b) MLS v5.0. Results are based on MLS H_2O profiles collocated with SAGE III/ISS and interpolated to a 0.5 km altitude grid. Time averaged thermal tropopause height calculated from the SAGE III/ISS temperature is over-plotted as gray solid lines. MLS, Microwave Limb Sounder; SAGE III/ISS, Stratospheric Aerosol and Gas Experiment III on the International Space Station.

at 1,022 nm as additional filters throughout this study to filter outliers. This filtering is stricter than what is used in Davis et al. (2021) and removes many of the obvious outliers in the upper troposphere and stratosphere. In Figure 1b, water vapor profiles with higher than 300% uncertainty or all points in a profile below the highest altitude at which the aerosol extinction coefficient at 1,022 nm exceeds $1 \times 10^{-3} \text{ km}^{-1}$ were removed. This screening filters most of the outliers in Figure 1a ($\sim 1.2\%$ of total data) and still preserves the majority of profiles. Figure 1b compares co-located profiles between SAGE III/ISS H_2O and MLS H_2O for measurements in the deep tropics (5°N – 5°S), after the filtering is applied to SAGE III/ISS, showing excellent agreement between ~ 17 and 30 km. SAGE III/ISS water vapor profiles exhibit more noise at lower altitudes (Figure 1a), which is related to aerosol/cloud interferences below ~ 20 km as discussed in Wang et al. (2020) and Davis et al. (2021). MLS water profiles also include a number of obvious outliers below the tropopause.

Global comparisons of SAGE III/ISS and both MLS v4.2 and v5.0 data are shown in Figures 2a and 2b based on the medians between June 2017 and November 2020. Time mean thermal tropopause height is calculated from the SAGE III/ISS temperature based on the temperature lapse rate (WMO, 1957). Comparisons with v4.2 show a $\sim 10\%$ dry bias in SAGE III/ISS (Figure 2a), as shown in Davis et al. (2021). The improvement in MLS v5.0 significantly reduces the median bias to a few percent (Figure 2b). The small differences in Figure 2b highlight exceptional overall agreement between the two very different satellite measurement techniques and retrievals. Overall, the agreement between SAGE III/ISS and MLS has been improved significantly in MLS v5.0 compared to MLS v4.2 due to changes in MLS v5.0 retrievals. The biases in Figures 2a and 2b do not show substantial latitudinal or vertical structure in the stratosphere except the small-scale features in the mid-stratosphere between ~ 30 and 45 km. Larger biases are found near and below the tropopause.

While there is good overall agreement between SAGE III/ISS v5.1 and MLS v5.0 stratospheric water vapor, there are times and regions where larger differences occur. For example, Figure 3a shows the difference between the two measurements in November 2019 where there are enhanced stratospheric aerosols from the Ulawun and Raikoke volcanic eruptions (Chouza et al., 2020; Kloss et al., 2021), as shown in the corresponding $1 \mu\text{m}$ aerosol extinction measured by SAGE III/ISS (Figure 3b). Figure 3a shows dry SAGE III/ISS water vapor biases of $\sim 5\%$ – 20% centered in the tropics and global lower stratosphere, approximately overlapping the enhanced aerosols in Figure 3b. There is also a wet bias in the SAGE III/ISS water vapor at the Northern Hemisphere (NH) high latitudes adjacent to Raikoke eruption. Similar anomalies in SAGE III/ISS water vapor are observed in conjunction with enhanced stratospheric aerosols from the Australian bush fires (Kablick et al., 2020) in early 2020 (not shown). This sensitivity of SAGE III/ISS stratospheric water vapor to elevated aerosol loading is discussed by Davis et al. (2021), which could be an artifact of the SAGE III/ISS water vapor retrieval algorithm. These affected SAGE III/ISS retrievals were not filtered by the stand-

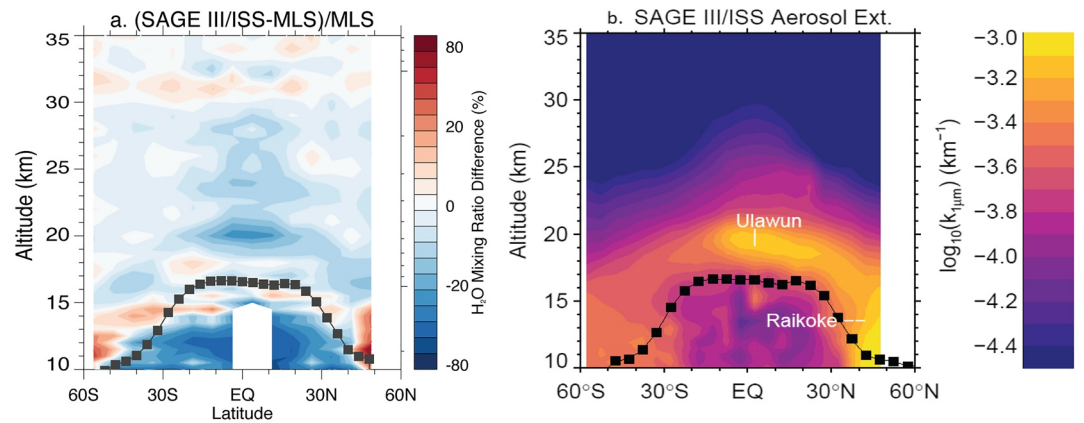


Figure 3. Latitude versus altitude sections of (a) Relative difference between SAGE III/ISS and MLS water vapor ($(\text{SAGE III/ISS-MLS/MLS} \times 100)$ averaged for November 2019 (unit: %). (b) Aerosol Extinction coefficients at 1,022 nm measured by SAGE III/ISS for the same month (unit: km^{-1}). Thermal tropopause height calculated from the SAGE III/ISS temperature is over-plotted as black solid lines with squares. MLS, Microwave Limb Sounder; SAGE III/ISS, Stratospheric Aerosol and Gas Experiment III on the International Space Station.

ard threshold values of retrieval uncertainty/aerosol optical depth discussed above, and more restrictive threshold values could be applied in these cases (with corresponding loss of SAGE III/ISS measurements), though such additional filtering is not explored here.

3.2. Near-Global Space-Time Variability

In the following, we examine large-scale behavior of water vapor observed by SAGE III/ISS including comparisons with MLS. SAGE III/ISS and MLS use different measurement techniques (solar occultation vs. microwave limb sounding) and have very different space-time sampling. While MLS makes $\sim 3,500$ measurements per day with near-global coverage (82°N – 82°S), SAGE III/ISS makes up to 31 sunrise and sunset occultation measurements per day and takes approximately one month to sample the region $\sim 60^\circ\text{N}$ – 60°S (see Figure 1 of Davis et al., 2021). The SAGE III/ISS measurements provide near-global longitudinal coverage of the tropics and middle latitudes for monthly averages, depending on the time of year.

As is well-known, the seasonal variation in water vapor entering the tropical lower stratosphere closely follows temperature near the tropical tropopause, setting the “base” for the so-called tropical tape recorder (Mote et al., 1996). Figure 4 shows the evolution of tropical (15°N – 15°S) water vapor over 2017–2020 observed by both SAGE III/ISS and MLS between 10 and 35 km altitude. Due to relatively sparse and uneven spatial sampling in SAGE III/ISS measurements, a smoothing is applied to SAGE III/ISS water vapor to fill the data gap and to reduce noise. As shown in Figure 4a, the number of data points vary depending on the season with the maxima in June (~ 90 profiles/6 days) and minima in December each year. First, the SAGE III/ISS water vapor profiles are averaged within the latitude bands every 6 days and then the Gaussian smoothing is applied at each altitude with the width of 18 days. The 6-day time average is applied to maintain the detailed temporal variability and to reduce the noise, while the Gaussian smoothing provides a smooth interpolation over data gaps in Figure 4a. The resulting fields are compared with daily data measured by MLS in Figure 4b. The observed variability in Figure 4 consists of boreal summer maxima (wet phase) and boreal winter minima (dry phase) originating near the tropical cold point tropopause (CPT), near ~ 17 km, propagating upwards to ~ 30 km with a phase lag of over one year. Overall, the SAGE III/ISS and MLS water vapor mixing ratios in Figure 4 show good agreement, with consistent phase and amplitude variations up to ~ 30 km. The SAGE III/ISS H_2O displays somewhat larger noise at upper levels due to low extinction signal from water vapor as discussed in Davis et al. (2021). It is interesting to note isolated maxima near 31 km in the MLS data centered on October–November each year in Figure 4b, which are not evident in the SAGE III/ISS data. In addition to the seasonal cycle, the water vapor minima and maxima in Figure 4 show consistent interannual changes between SAGE III/ISS and MLS. For instance, both instruments show the dry phase in early 2019 is drier than in 2018 and 2020, and the wet phase during

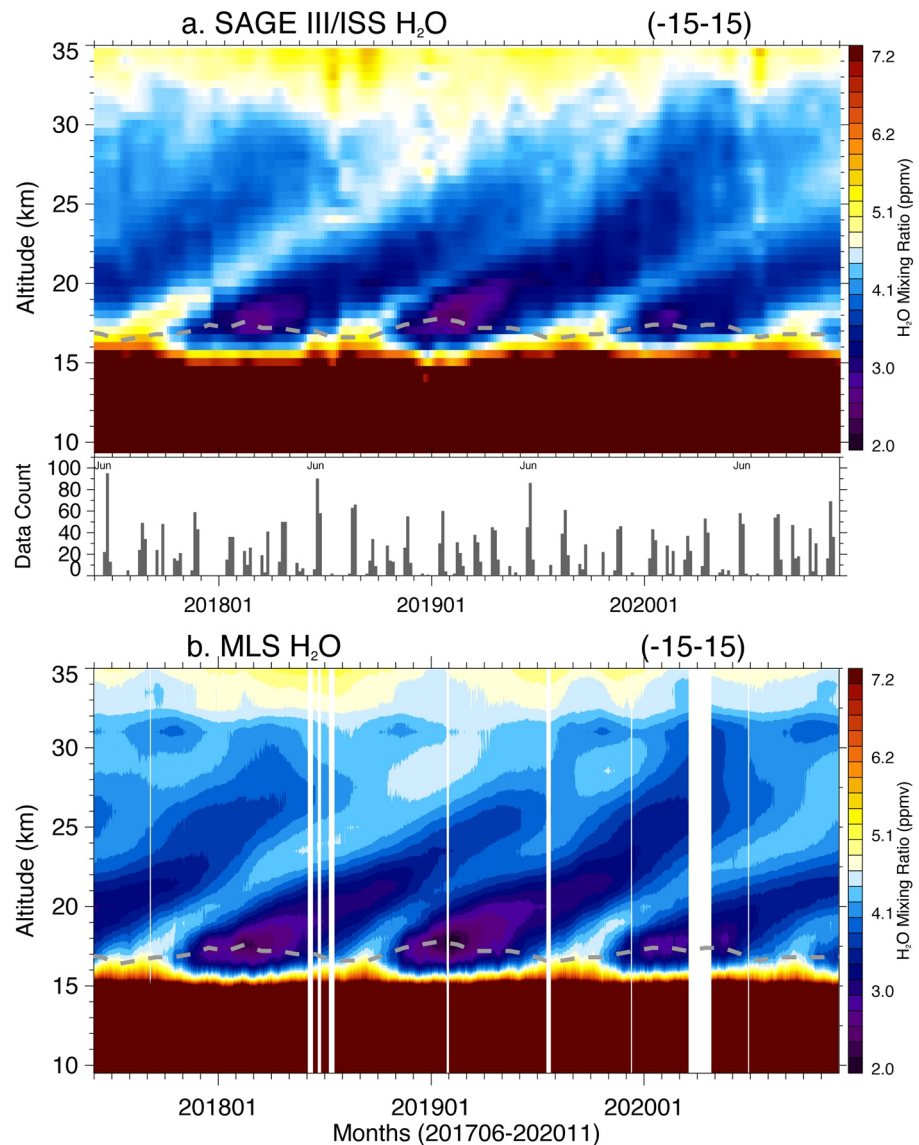


Figure 4. Time versus altitude sections of zonal average water vapor mixing ratios (unit: ppmv) observed from (a) SAGE III/ISS and (b) MLS for June 2017 to November 2020 averaged between 15°S and 15°N latitude. The SAGE III/ISS data are averaged every 6 days and a Gaussian smoothing is applied to the averaged profiles with time in (a). The number of SAGE III/ISS profiles used in 6-day averages is shown at the bottom panel in (a). The MLS water vapor daily averaged data are shown in altitude grids in (b). Dark gray dashed lines denote cold point tropopause height derived from the GPS temperature between 15°S and 15°N latitude. MLS, Microwave Limb Sounder; SAGE III/ISS, Stratospheric Aerosol and Gas Experiment III on the International Space Station.

boreal summer of 2017 is wetter than in the summer of 2018. The wet phase maximum in the summer of 2019 is close to the one in 2017 for MLS, but this behavior is less clear from SAGE III/ISS data because of data voids related to enhanced stratospheric aerosols in this year. The interannual variations originating near the tropopause propagate coherently into the stratosphere, which is typical behavior observed in the longer-term MLS data record (e.g., Randel & Park, 2019).

The evolution of global water vapor measured by SAGE III/ISS demonstrates transport processes associated with tape recorder development from the boreal summer into winter. The moist phase of the tape recorder is related to relatively warm tropical tropopause temperatures, in addition to contribution via transport from the boreal summer monsoons (e.g., Bannister et al., 2004; Nutzel et al., 2019; Yu et al., 2020). Clear evidence of this latter behavior is provided by the high vertical resolution SAGE III/ISS data during the summer in

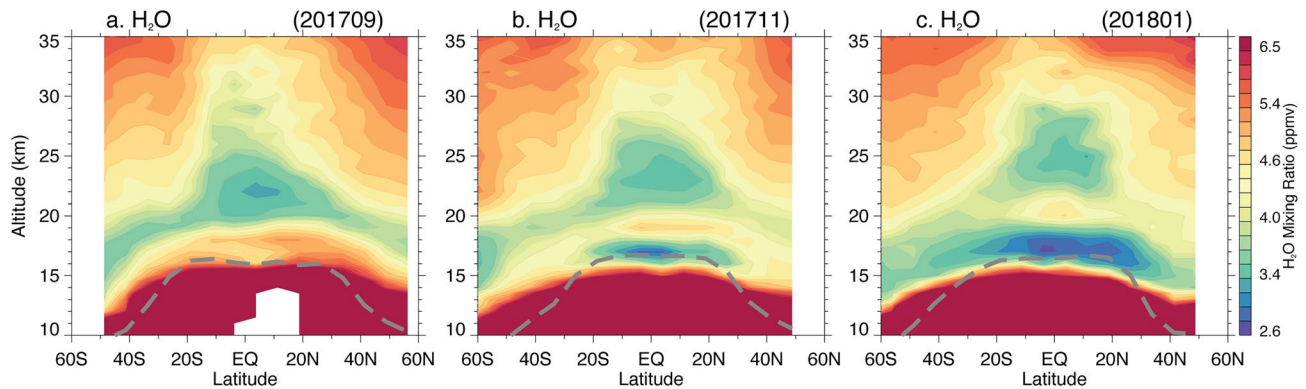


Figure 5. Zonal mean monthly average water vapor mixing ratios (unit: ppmv) obtained from SAGE III/ISS for (a) September 2017, (b) November 2017, and (c) January 2018. The thermal tropopause derived from the SAGE III/ISS temperature is shown as thick gray dashed lines. SAGE III/ISS, Stratospheric Aerosol and Gas Experiment III on the International Space Station.

2017 into winter in 2018 in Figure 5. A lower stratosphere water vapor maximum over the NH subtropics (~15–18 km) tied to the monsoons propagates upwards and equatorward in a narrow layer and contributes to the moist phase of the tape recorder over the equator several months later. By November 2017, a thin layer of relatively higher water vapor exists between 18 and 20 km in the tropics (Figure 5b) while a water vapor minimum forms near the tropical tropopause. The water vapor minimum is widespread in latitude during January 2018 (Figure 5c). The time evolution shown in Figure 5 highlights well-known aspects of water vapor including origination of the dry phase near the equatorial tropopause and rapid global transport to high latitudes within the lowest stratosphere, and isolation of air in the “tropical pipe” above ~22 km.

Water vapor variability in the lower stratosphere (~18 km) over 60°N–60°S highlights strong seasonality and equator to pole meridional transport (Figure 6). Figure 6a shows daily average water vapor measurements at 18 km from SAGE III/ISS with a Gaussian smoothing applied with time, compared in Figure 6b with MLS daily H₂O data interpolated to 18 km. The strong annual cycle occurs in the tropics over ~20°N–20°S, with low water vapor mixing ratios centered over the equator in winter and high values over ~0–30°N in summer, the latter associated with the boreal summer monsoon circulations. In both cases, the water vapor extrema in low latitudes propagate to high latitudes and this is especially clear for the transport to the Arctic during summer (as simulated in Ploeger et al., 2013). These patterns are evident in the SAGE III/ISS and MLS water vapor measurements, including consistent year-to-year variations. For instance, the water vapor maxima in the NH summer are higher in 2017 and the tropical minima are lower during early 2019. SAGE III/ISS data in Figure 6a display somewhat sparser sampling during 2019–2020 related to the loss of data due to enhanced stratospheric aerosol loadings, as discussed above.

3.3. Seasonal Variability in the UTLS

Much of the seasonal changes in longitudinal structure in stratospheric water vapor occurs in the UTLS region, and comparisons of water vapor distributions between SAGE III/ISS and MLS for NH summer and winter of 2017–2018 in the UTLS are shown in Figure 7. August and January are chosen to represent the NH summer and winter respectively as SAGE III/ISS provides near-global coverage (60°S–60°N) in those months of each year. Individual profiles of SAGE III/ISS H₂O are gridded at 15° × 7.5° (longitude × latitude) grids using the available observations during August 2017 and January 2018. SAGE III/ISS measurement locations are indicated in Figures 7a and 7c. For comparison, the MLS monthly average is constructed on the same horizontal grid as shown in Figures 7b and 7d. The comparisons in Figure 7 show reasonable agreement between SAGE III/ISS and MLS in terms of spatial structure, in spite of the limited SAGE III/ISS sampling. For boreal summer (Figures 7a and 7b), 16.5 km is close to the local tropical tropopause, where water vapor shows the maxima over the Asian and North American monsoons, in addition to a maximum west of equatorial Africa. Comparisons in January 2018 (Figures 7c and 7d) at 18 km (close to the cold point tropopause in boreal winter) show consistent water vapor minima over the tropical western Pacific, albeit with some differences in detailed spatial structure. Overall, the comparisons shown in Figure 7 and other

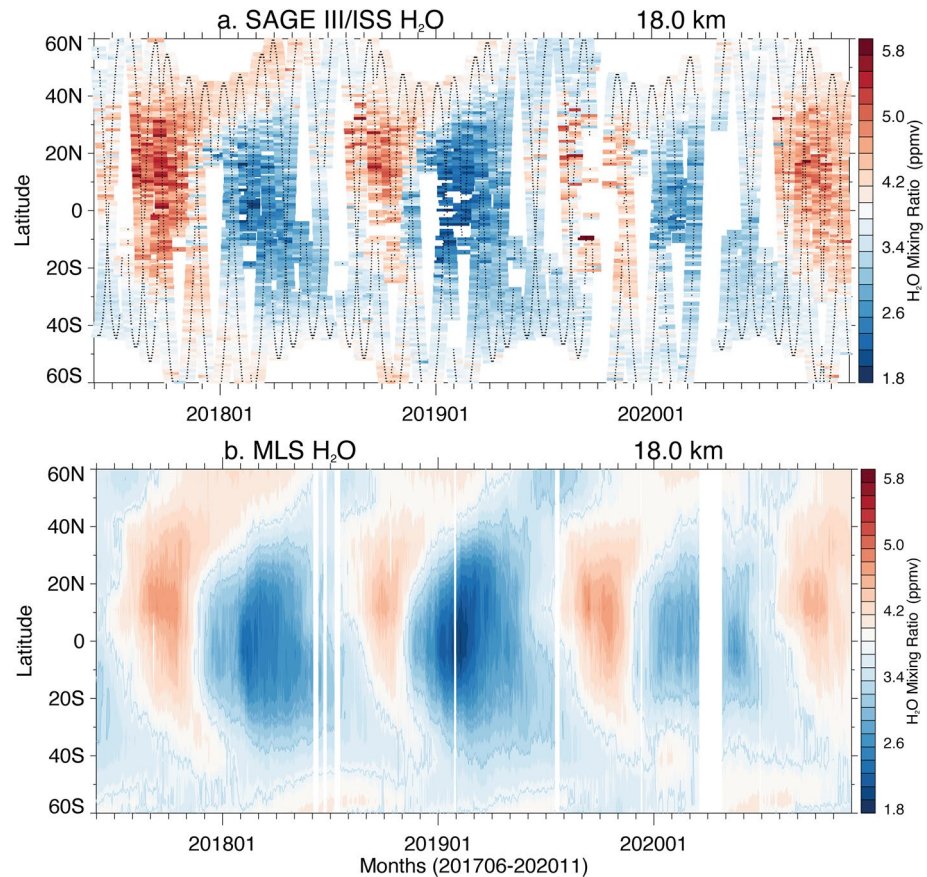


Figure 6. Time versus latitude sections of zonal average water vapor mixing ratios (unit: ppmv) obtained from (a) SAGE III/ISS gridded with the Gaussian smoothing and (b) MLS daily data interpolated to 18 km altitude from June 2017 to May 2020. Black dots in (a) represent SAGE III/ISS daily data locations without the Gaussian smoothing. MLS, Microwave Limb Sounder; SAGE III/ISS, Stratospheric Aerosol and Gas Experiment III on the International Space Station.

months (not shown) show reasonable agreement between SAGE III/ISS and MLS water vapor sampled at monthly cadence, highlighting the capability of SAGE III/ISS to monitor stratospheric water vapor structure and variability on monthly and seasonal time scales. Note, the latitudinal coverage of the SAGE III/ISS measurements varies by season due to its orbit (see Figure 6a).

As is well-known, during NH summer enhanced water vapor mixing ratios are observed near the tropopause over the Asian and North American (NA) monsoon regions, including occasional high values (above 8 ppmv) possibly linked with extreme convection (Jensen et al., 2020; Schwartz et al., 2013; Smith et al., 2017). During August 2017, the water vapor maxima over the NA monsoon was relatively higher than over the Asian monsoon (Figures 7a and 7b). This is considered to be a typical behavior and there exists substantial year-to-year variability (Randel et al., 2015). To explore vertical structure over the monsoon regions, and its variability, Figures 8a and 8b show time average vertical profiles of water vapor and co-located temperature profiles over both the monsoon regions (marked as boxes in Figures 7a and 7b) for each August of the 4 years (2017–2020). The average water vapor profile over NA in August 2017 shows higher values between 16 and 19 km compared to the other years, and also compared to all 4 years over the Asian monsoon region. The average temperatures are generally warmer and have larger interannual variability over NA compared to over Asia, and there are not obvious relationships between time average water vapor and co-located temperature profiles. Interestingly, the August 2017 temperatures over NA are relatively cold while the water vapor is relatively high, which demonstrates that local temperatures are not controlling water vapor. The relatively high water vapor values in August 2017 are consistent with higher values during the wet phase of the tropical tape recorder seen in Figure 4a. Over the Asian monsoon region, lower temper-

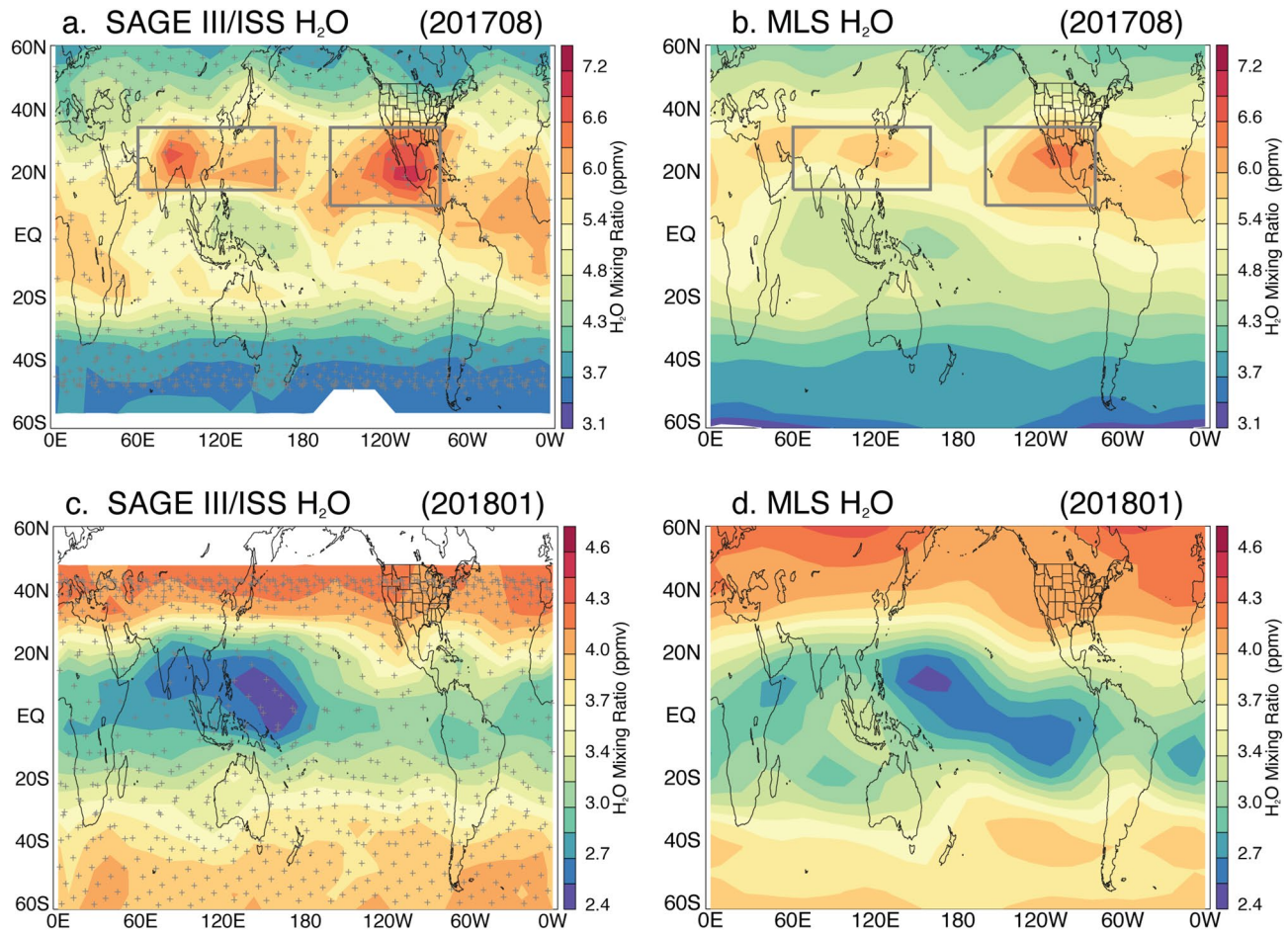


Figure 7. Longitude versus latitude sections of (a and c) SAGE III/ISS and (b and d) MLS water vapor (unit: ppmv) for (top) August 2017 at 16.5 km and (bottom) January 2018 at 18.0 km, respectively. Locations of SAGE III/ISS measurements during these months are marked as gray plus signs in (a and c). Gray solid lines in (a and b) represent the Asian (60° – 160° E longitude/ 15° – 35° N latitude) and North American (160° – 80° W longitude/ 10° – 35° N latitude) monsoon regions, respectively. Note, the color scales are different between the summer and the winter months. MLS, Microwave Limb Sounder; SAGE III/ISS, Stratospheric Aerosol and Gas Experiment III on the International Space Station.

atures with higher hygropauses exist and the water vapor profiles do not show significant changes among those 4 years.

We further examine the individual SAGE III/ISS water vapor profiles and relationships to co-located temperatures over the Asian and NA monsoon regions. Figures 8c and 8d show all of the individual measurements of water vapor and temperature between ~ 15.5 and 21.5 km during August 2017 and August 2018. Those 2 years are chosen as examples of extreme years from Figure 8b. August 2017 shows highest water and coldest average temperatures, and August 2018 shows warmest temperatures over the NA. The data points in Figures 8c and 8d are color coded according to altitude, and the red points highlight measurements above the local CPT with temperatures below 200 K. Over the Asian monsoon, a few points with very low water vapor mixing ratios (~ 3 ppmv) exist with very low temperatures (< 197 K) near ~ 17 km. Over North America, higher water vapor mixing ratios coexist with higher temperatures up to ~ 18 km, which is above the CPT. Points above the local CPT with higher water vapor mixing ratios and low temperatures (< 200 K) are most common over North America in August 2017. Figures 8c and 8d also include the corresponding saturation mixing ratios (q_{SAT}) calculated from the observed temperatures for comparison to observed water vapor. The key feature in these results is that observed water vapor is well below saturation throughout both monsoon regions, aside from a few individual points close to the tropopause in the NA monsoon in August 2017. These results showing sub-saturation from SAGE III/ISS measurements are consistent with climatologies of relative humidity in the monsoon regions derived from MLS and Atmospheric Chemistry

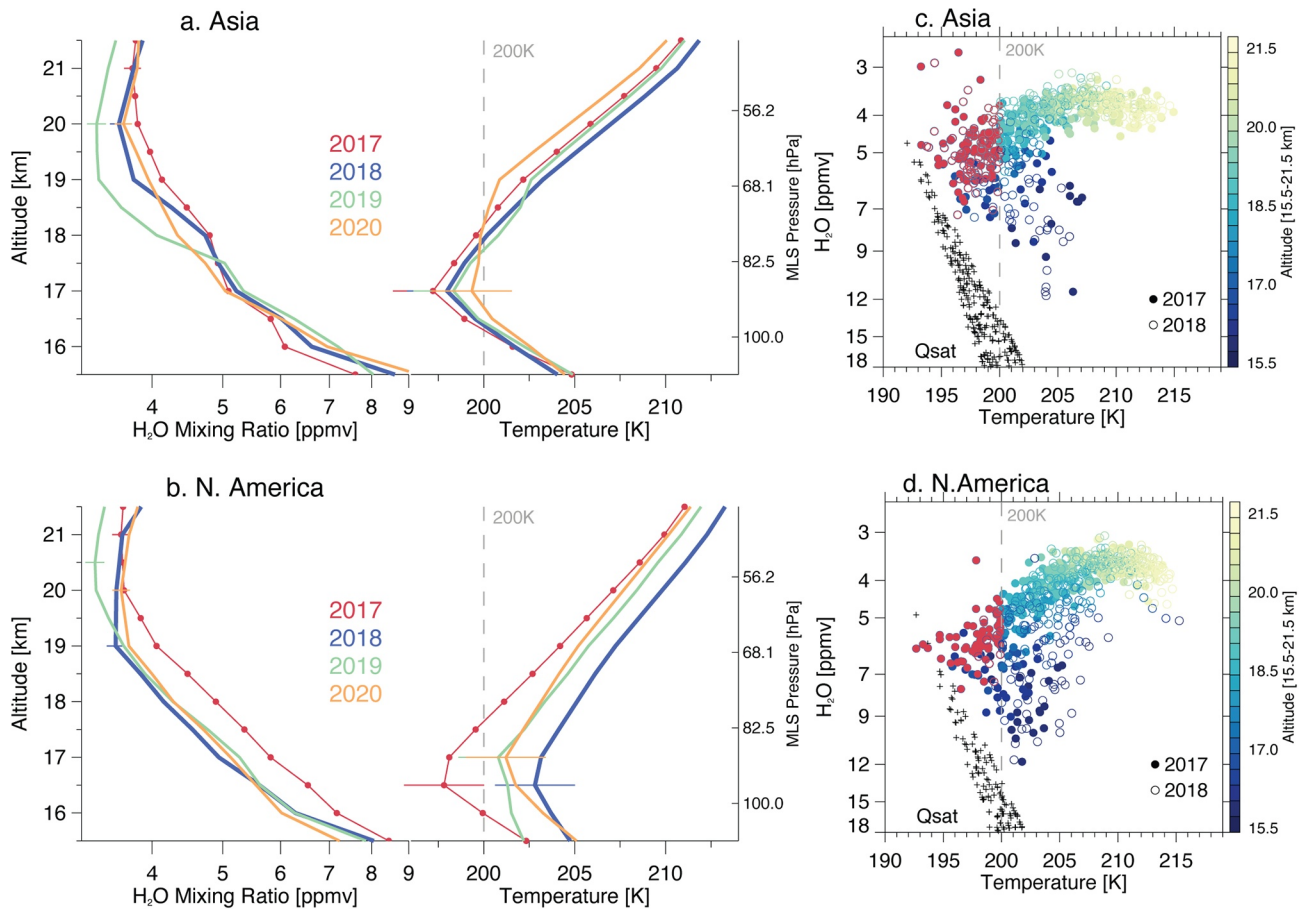


Figure 8. Vertical profiles of water vapor mixing ratios (unit: ppmv) and temperature averaged over (a) Asia (60° – 160° E/ 15° – 35° N) and (b) North America (160° – 80° W/ 10° – 35° N) for August 2017–2020. August 2017 is shown as solid lines with filled circles and August 2018 is shown as solid blue lines. Hygropauses in each average water vapor profile and cold point tropopauses are marked as horizontal lines in (a and b). Gray dashed lines mark 200 K temperature in (a and b). Scatter plots of water vapor versus temperature between 15.5 and 21.5 km over (c) Asia and (d) North America for August 2017 (filled circles) and 2018 (open circles). Red filled (2017) and open (2018) circles indicate SAGE III/ISS water vapor measurements above the local cold point tropopause with low temperature ($T < 200$ K, shown as gray dashed lines). q_{SAT} values for the corresponding temperature and pressure of individual data points are over-plotted as small black plus signs in (c and d). Colors indicate altitude of individual profiles (15.5–21.5 km). SAGE III/ISS, Stratospheric Aerosol and Gas Experiment III on the International Space Station.

Experiment-Fourier Transform Spectrometer (ACE-FTS) water vapor measurements (for details, see Randel et al., 2012). We note that while water vapor near and above the CPT is higher over NA compared to Asia in Figures 8c and 8d, there are no individual extreme values above 8 ppmv in the SAGE III/ISS measurements (in all 4 years, not shown). However, that is not surprising given their infrequent occurrence (less than 1%) in MLS data as shown in Schwartz et al. (2013).

3.4. UTLS Relative Humidity

We include analysis of climatological relative humidity derived from SAGE III/ISS water vapor retrievals combined with co-located temperatures from MERRA-2 (Gelaro et al., 2017). Evaluating the RH distribution near the tropical tropopause from satellite data is valuable for identification of large-scale structure and regions near saturation that have implications for stratospheric dehydration and cirrus formation. However, there are important caveats regarding the evaluation of RH from SAGE III/ISS solar occultation data. First, it is important to note that SAGE III/ISS water vapor retrievals are affected by the presence of opaque convective clouds or cirrus clouds near the tropical tropopause. This is true both within and below the clouds where the water vapor signal becomes weak or the inversion process fails (see Davis

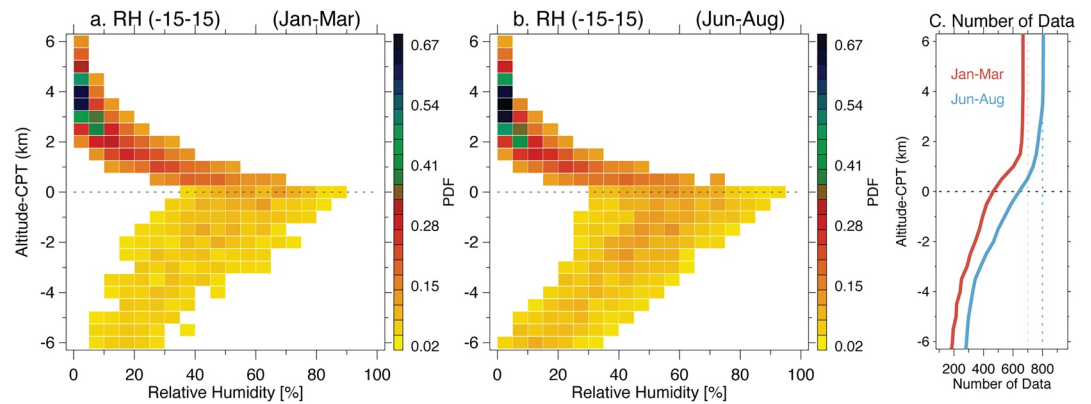


Figure 9. PDFs of relative humidity versus altitude relative to the cold point tropopause calculated from SAGE III/ISS water vapor and MERRA-2 temperature profiles between 15°S and 15°N, for statistics during (a) January–March (2018–2020) and (b) June–August (2017–2019). (c) The corresponding number of measurements at each altitude for January–March (red) and June–August (blue). Thin red and blue dotted lines mark 700 and 800 for references, respectively. PDFs, probability density functions; SAGE III/ISS, Stratospheric Aerosol and Gas Experiment III on the International Space Station.

et al., (2021) for details). As a result, more reliable water vapor retrievals and the derived RH statistics primarily represent clear-sky areas, which is known to have lower RH than cloudy areas (e.g., Jensen et al., 2017; Kahn et al., 2009; Krämer et al., 2020). The loss of SAGE III/ISS measurements due to clouds is quantified below by showing the number of measurements as a function of altitude relative to the tropopause. A second point is that the spatial structure of RH near the tropopause often exhibits small horizontal and vertical scales (e.g., Jensen et al., 2013), often typically associated with small-scale waves (Jensen & Pfister, 2004; Kim et al., 2016; Ueyama et al., 2015). Satellite measurements provide a large-scale three-dimensional integrated perspective on the relevant moisture and temperature fields, averaged over ~ 200 km horizontally and ~ 1 km vertically in the case of SAGE III/ISS water vapor. Such satellite measurements cannot identify localized regions of supersaturation as observed in aircraft measurements (e.g., Jensen et al., 2017; Krämer et al., 2020), but rather are useful to provide a global perspective to the high-resolution in situ measurements.

We calculate RH with respect to ice from the ratio: $RH = (q/q_{SAT}) \times 100\%$, where q is the SAGE III/ISS water vapor mixing ratio and q_{SAT} is the saturation mixing ratio over ice calculated from the MERRA-2 temperature profiles based on Murphy and Koop (2005). We use the MERRA-2 temperature profiles linked with the DMPs (Manney et al., 2007, 2011), which provide higher vertical resolution (72 vertical levels, UTLS resolution of ~ 0.7 km) compared to the lower resolution temperature profiles (47 levels) provided with the SAGE III/ISS retrievals. Because of relatively large uncertainty in the RH calculated from individual profiles and the sampling considerations discussed above, we focus on the statistical behavior of RH in the tropics throughout the seasonal cycle, and in the boreal summer monsoon regions (primarily representing clear-sky areas, as noted above). We organize the vertical structure of RH with respect to the cold point tropopause observed in each profile.

The statistical distribution of RH in the deep tropics (15°N–15°S) as a function of altitude relative to the cold point tropopause is shown for boreal winter (January–March; “cold” season) and summer (June–August; “warm” season) in Figures 9a and 9b. The corresponding total number of measurements at each altitude for each season is shown in Figure 9c, illustrating the significant drop-off of measurements at and below the tropopause, due to cloud effects noted above. Hence the RH statistics in Figures 9a and 9b mainly reflect clear-sky (lower RH) conditions. The RH distributions in Figure 9 show generally increasing RH up to the cold point, as expected, with RH decreasing quickly with altitude into the lower stratosphere. The peak of the RH distributions at the cold point occurs for RH $\sim 40\%$ – 70% for both seasons, with a relatively small difference in the distribution between these seasons. We note that the vertical structures in Figure 9 are similar to RH statistics derived from MLS measurements presented in Schoeberl et al. (2019), but with improved vertical resolution provided by SAGE III/ISS.

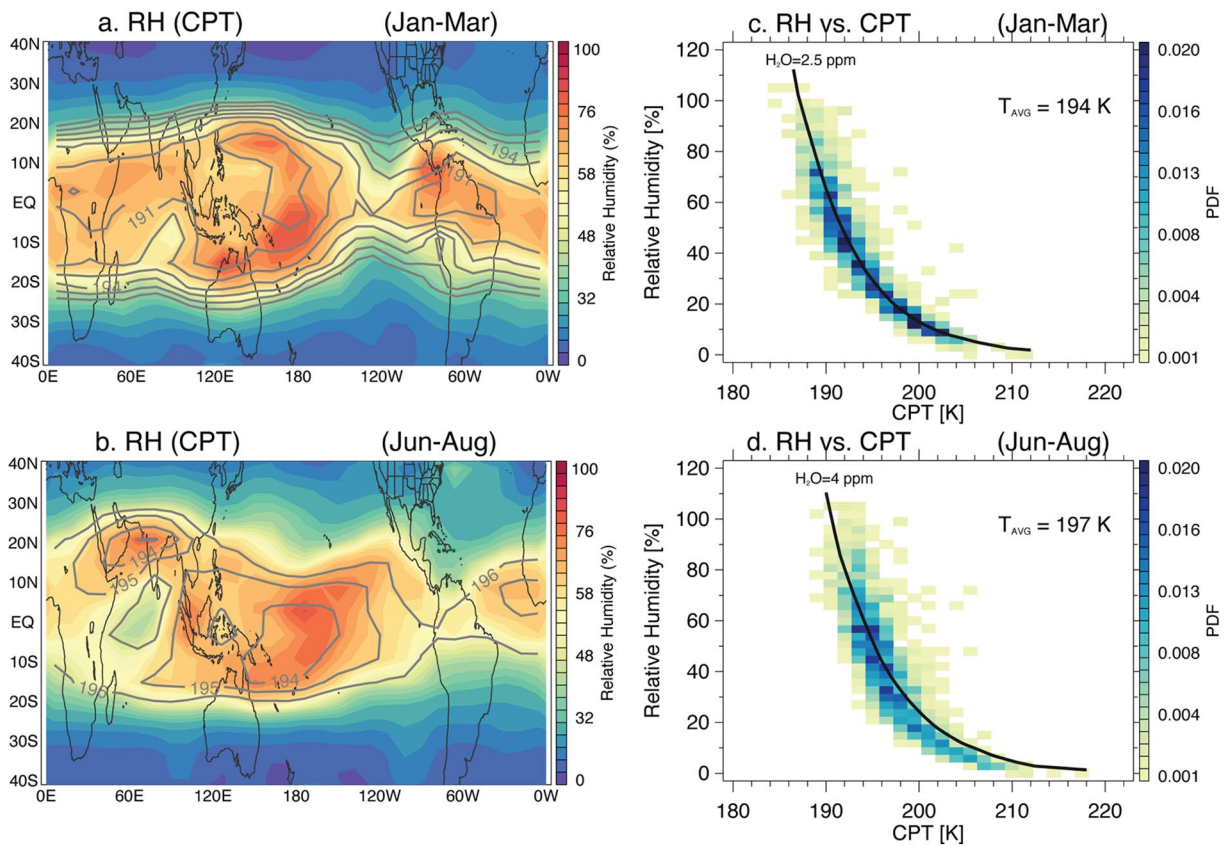


Figure 10. Climatological structure of RH at the local CPT derived from all SAGE III/ISS H₂O and temperature measurements averaged during (a) January–March (2018–2020) and (b) June–August (2017–2019). Climatological CPT temperatures averaged for the same periods are overlaid as gray solid lines (contours are only shown for $T < 196$ K). (c and d) PDFs of corresponding RH versus CPT for the two seasons from all of the individual measurements over 30°N–30°S. Time average CPT temperatures for each season between 30°N and 30°S are noted in (c and d). Black solid lines show RH versus CPT for constant H₂O mixing ratios (2.5 and 4 ppm for (c and d), respectively). Temperature and pressure from the SAGE III/ISS data are used in this calculation. CPT, cold point tropopause; PDFs, probability density functions; SAGE III/ISS, Stratospheric Aerosol and Gas Experiment III on the International Space Station.

We have evaluated the distribution of RH at the tropical cold point throughout the SAGE III/ISS record over 2017–2020 based on the approximate monthly sampling of the tropics (not shown). While H₂O shows the well-known tropical annual cycle in response to varying tropopause temperatures (e.g., Figures 4 and 6), the RH values do not show a systematic seasonal variation, but rather distributions similar to Figures 9a and 9b (with maxima spanning RH ~40%–70% at the cold point) throughout the year. We have also evaluated the RH distributions in the Asian and North American monsoon regions, in light of enhanced H₂O in these regions (e.g., Figure 7a). Statistics show higher overall RH in the Asian monsoon compared to the North American monsoon, although both are well undersaturated (in clear-sky regions), as inferred from Figures 8c and 8d. RH over the Asian monsoon region shows a close resemblance to the distribution in the tropics in winter and summer (not shown).

Time average maps of RH at the cold point for the NH winter (cold) and summer (warm) seasons are shown in Figures 10a and 10b, constructed from all available measurements from SAGE III/ISS over 2018–2020. Time averaged CPT temperatures are over-plotted for each season based on the co-located temperature profiles, showing the well-known seasonally evolving climatological structure (e.g., Kim & Son, 2012; Schoeberl et al., 2019). The lowest temperature occurs over the Western Pacific in winter (Figure 10a) and over the Central Pacific and Asian monsoon region in summer (Figure 10b). Enhanced RH is observed over the Pacific in both seasons, generally co-located with coldest temperatures. Additional RH maxima occur in boreal winter in cold tropopause regions including South America and east of Africa. Boreal summer exhibits a localized RH maximum over the cold southern flank of the Asian monsoon region in Figure 10b (near 20°N, 60°E), and this behavior is consistent with this region controlling H₂O in the Asian monsoon by

horizontal circulation through the cold region (Randel et al., 2015; Ueyama et al., 2018; Wright et al., 2011). Note that there is no clear indication of an RH maximum co-located with a temperature minimum over the North American monsoon region in the SAGE III/ISS statistics in Figure 10b, which suggests weaker links between RH and temperature in this region.

Statistical relationships between RH and CPT temperature for the tropical SAGE III/ISS data are shown in Figures 10c and 10d for the two seasons, based on individual measurement between 30°N and 30°S for January (2018–2020) and August (2017–2019). The PDFs demonstrate compact relationships between RH and CPT, with high RH occurring in the coldest regions in both the seasons. The average CPT temperature is lower in NH winter (194 K) than in summer (197 K) for the similar RH distributions. In NH winter (Figure 10c), the distribution closely follows the constant H₂O mixing ratio curve (2.5 ppm). This compact relationship suggests that water vapor has a very small influence in controlling relative humidity in this region. Instead, temperature at the local CPT controls relative humidity in the tropics. In NH summer (Figure 10d), the RH distribution follows the higher H₂O mixing ratio curve (4 ppm) and shows a compact relationship similar to the NH winter. When the RH is lower than 20%, the PDFs distribution is centered below the 4-ppm curve, which needs further investigation. These RH-temperature relationships are in quantitative agreement with near-tropopause statistics derived from high resolution aircraft measurements (for clear-sky, e.g., Figure 5b in Jensen et al., 2017 and Figure 6 in Krämer et al., 2020). This agreement enhances confidence in the climatological statistics derived from SAGE III/ISS. The PDFs distributions for the individual years show consistent behavior with the climatology shown here (figure not shown).

4. Summary and Discussion

In this work, we evaluated the large-scale geophysical variability in the first 3 years of SAGE III/ISS v5.1 water vapor data. Our goal is to validate water vapor measurements from SAGE III/ISS against other satellite measurements qualitatively and also evaluate global and seasonal variability for scientific studies. The SAGE III/ISS water vapor shows expected seasonal variability, including the well-known “tape recorder” in the tropical stratosphere (Figure 3). The tropical annual cycle originating near the cold point tropopause propagates both upward in the tropics and poleward in both hemispheres of the lower stratosphere (Figure 5, the “horizontal tape recorder”). The comparisons between SAGE III/ISS and MLS v5.0 show excellent overall agreement between the two data sets from the tropopause through the middle stratosphere (~16–30 km). The high vertical resolution SAGE III/ISS data provide an excellent demonstration of lower stratospheric water vapor maxima associated with the boreal summer monsoons that propagate to the tropics and contribute to the moist phase of the tape recorder (Figure 4). While the SAGE III/ISS sampling takes approximately one month to cover the latitude range ~60°N–60°S, we find that monthly sampling captures the essential longitudinal structure of water vapor in the lower stratosphere, including localized maxima tied to the summer monsoons and minima over the Western Pacific in the winter (Figure 6). Comparisons with MLS also demonstrate that SAGE III/ISS can accurately capture interannual variations in stratospheric water vapor. For instance, the water vapor minima in the tropics and the maxima over the NH subtropics associated with the summer monsoons vary year-by-year, which are key for evaluating the related physical processes. Overall, these comparisons demonstrate that SAGE III/ISS sampling and data quality are adequate for monitoring stratospheric water vapor variability and changes. The SAGE III/ISS water vapor retrievals show higher sensitivity to enhanced stratospheric aerosol loadings during the events of volcanic eruptions (Chouza et al., 2020; Kloss et al., 2021) and wildfires (Kablick et al., 2020). We have applied stricter filtering criteria to remove the outliers and caution is needed in filtering the data in these extreme events (see, Davis et al., 2021 for details).

We have used the high vertical resolution SAGE III/ISS water vapor data together with co-located MERRA-2 temperatures to evaluate large-scale relative humidity behavior in the tropics, with the caveat that these data primarily represent clear-sky regions. Results show that RH increases in the upper troposphere up to the cold point (as expected), with maximum RH distribution around ~40%–70% at the cold point. There are not obvious seasonal variations in this statistical RH distribution in the deep tropics during the year, in spite of clear annual cycles in temperature and water vapor. Spatial distributions of RH at the cold point tropopause during the solstice seasons (Figures 10a and 10b) show a close link between RH and large-scale temperature, with statistical relationships (Figures 10c and 10d) that are in good agreement with (clear-sky)

UTLS aircraft measurements (Jensen et al., 2017; Krämer et al., 2020). This behavior enhances confidence in the overall quality of the SAGE III/ISS water vapor data and suggests these data can be useful for more detailed studies of RH distribution and variability, and for constraining global model behavior. Additionally, quantitative analyses of sampling biases between SAGE III/ISS and other satellite instruments as shown in Millán et al. (2016) will be beneficial in assessing changes in the stratosphere.

Data Availability Statement

The SAGE III/ISS v5.1 water vapor data and the Aura MLS water vapor v5.0 data are publicly available through the NASA Goddard Earth Sciences Data and Information Services Center (GES DISC). The SAGE III/ISS L2 Solar Event Species Profiles (HDF-EOS) V051 can be obtained from https://dx.doi.org/10.5067/ISS/SAGEIII/SOLAR_HDF4_L2-V5.1. The Aura MLS water vapor v5.0 data sets are available in the following link <https://dx.doi.org/10.5067/Aura/MLS/DATA2508>. The MERRA-2 temperature included in the DMPs is available in the following link <https://mls.jpl.nasa.gov/dmp/>

Acknowledgments

The authors thank Eric Jensen and Ren Smith for their helpful comments on the manuscript. SAGE III/ISS is a NASA Langley managed Mission funded by the NASA Science Mission Directorate within the Earth Systematic Mission Program. Enabling partners are the NASA Human Exploration and Operations Mission Directorate, International Space Station Program and the European Space Agency. Work at the Jet Propulsion Laboratory, California Institute of Technology, was carried out under a contract with the National Aeronautics and Space Administration. The National Center for Atmospheric Research is operated by the University Corporation for Atmospheric Research, under sponsorship of the National Science Foundation. Any opinions, findings, and conclusions or recommendations expressed in this publication are those of the author(s) and do not necessarily reflect the views of the National Science Foundation.

References

- Anderson, J. G., Wilmouth, D. M., Smith, J. B., & Sayres, D. S. (2012). UV dosage levels in summer: Increased risk of ozone loss from convectively injected water vapor. *Science*, 337, 835–839. <https://doi.org/10.1126/science.1222978>
- Avery, M. A., Davis, S. M., Rosenlof, K. H., Ye, H., & Dessler, A. E. (2017). Large anomalies in lower stratospheric water vapour and ice during the 2015–2016 El Niño. *Nature Geoscience*, 10(6), 405–409. <https://doi.org/10.1038/ngeo2961>
- Banerjee, A., Chiodo, G., Previdi, M., Ponater, M., Conley, A. J., & Polvani, L. M. (2019). Stratospheric water vapor: An important climate feedback. *Climate Dynamics*, 53, 1697–1710. <https://doi.org/10.1007/s00382-019-04721-4>
- Bannister, R. N., O’neill, A., Gregory, A. R., & Nissen, K. M. (2004). The role of the south-east Asian monsoon and other seasonal features in creating the ‘tape-recorder’ signal in the Unified Model. *Quarterly Journal of the Royal Meteorological Society*, 130, 1531–1554. <https://doi.org/10.1256/qj.03.106>
- Bernath, P. F., McElroy, C. T., Abrams, M. C., Boone, C. D., Butler, M., Camy-Peyret, C., et al. (2005). Atmospheric chemistry experiment (ACE): Mission overview. *Geophysical Research Letters*, 32, L15S01. <https://doi.org/10.1029/2005gl022386>
- Boone, C. D., Bernath, P. F., Cok, D., Jones, S. C., & Steffen, J. (2020). Version 4 retrievals for the atmospheric chemistry experiment Fourier transform spectrometer (ACE-FTS) and imagers. *Journal of Quantitative Spectroscopy and Radiative Transfer*, 247, 106939. <https://doi.org/10.1016/j.jqsrt.2020.106939>
- Chouza, F., Leblanc, T., Barnes, J., Brewer, M., Wang, P., & Koon, D. (2020). Long-term (1999–2019) variability of stratospheric aerosol over Mauna Loa, Hawaii, as seen by two co-located lidars and satellite measurements. *Atmospheric Chemistry and Physics*, 20, 6821–6839. <https://doi.org/10.5194/acp-20-6821-2020>
- Chu, W. P., & Veiga, R. (1998). SAGE III/EOS. Proceedings of SPIE 3501, Optical Remote Sensing of the Atmosphere and Clouds. <https://doi.org/10.1117/12.577943>
- Cisevski, M., Zawodny, J., Gasbarre, J., Eckman, R., Topiwala, N., Rodriguez-Alvarez, O., et al. (2014). *The Stratospheric Aerosol and Gas Experiment (SAGE III) on the International Space Station (ISS) Mission*. Proceedings of SPIE 9241, Sensors, Systems, and Next-Generation Satellites XVIII, 924107. <https://doi.org/10.1117/12.2073131>
- Damadeo, R. P., Zawodny, J. M., Thomason, L. W., & Iyer, N. (2013). SAGE version 7.0 algorithm: Application to SAGE II. *Atmospheric Measurement Techniques*, 6, 3539–3561. <https://doi.org/10.5194/amt-6-3539-2013>
- Davis, S. M., Damadeo, R., Flittner, D., Rosenlof, K. H., Park, M., Randel, W. J., et al. (2021). Validation of SAGE III/ISS solar water vapor data with correlative satellite and balloon-borne measurements. *Journal of Geophysical Research: Atmospheres*, 125, e2020JD033803. <https://doi.org/10.1029/2020JD033803>
- Davis, S. M., Rosenlof, K. H., Hassler, B., Hurst, D. F., Read, W. G., Vömel, H., et al. (2016). The Stratospheric Water and Ozone Satellite Homogenized (SWOOSH) database: A long-term database for climate studies. *Earth System Science Data*, 8, 461–490. <https://doi.org/10.5194/essd-8-461-2016>
- Dessler, A. E., Schoeberl, M. R., Wang, T., Davis, S. M., & Rosenlof, K. H. (2013). Stratospheric water vapor feedback. *Proceedings of the National Academy of Sciences of the United States of America*, 110(45), 18087–18091. <https://doi.org/10.1073/pnas.1310344110>
- Forster, P. M. F., & Shine, K. P. (2002). Assessing the climate impact of trends in stratospheric water vapor. *Geophysical Research Letters*, 29(6). <https://doi.org/10.1029/2001gl013909>
- Fromm, M., Lindsey, D. T., Servranckx, R., Yue, G., Trickl, T., Sica, R., et al. (2010). The untold story of pyrocumulonimbus. *Bulletin of the American Meteorological Society*, 91, 1193–1210. <https://doi.org/10.1175/2010bams3004.1>
- Gelaro, R., Suárez, W. M. J., Todling, R., Molod, A., Takacs, L., Randles, C. A., et al. (2017). The modern-era retrospective analysis for research and applications, version 2 (MERRA-2). *Journal of Climate*, 30, 5419–5454. <https://doi.org/10.1175/jcli-d-16-0758.1>
- Hurst, D. F., Read, W. G., Vömel, H., Selkirk, H. B., Rosenlof, K. H., Davis, S. M., et al. (2016). Recent divergences in stratospheric water vapor measurements by frost point hygrometers and the Aura Microwave Limb Sounder. *Atmospheric Measurement Techniques*, 9, 4447–4457. <https://doi.org/10.5194/amt-9-4447-2016>
- Jensen, E. J., Lawson, R. P., Bergman, J. W., Pfister, L., Bui, T. P., & Schmitt, C. G. (2013). Physical processes controlling ice concentrations in synoptically forced, midlatitude cirrus. *Journal of Geophysical Research: Atmospheres*, 118, 5348–5360. <https://doi.org/10.1002/jgrd.50421>
- Jensen, E. J., Pan, L. L., Honomichl, S., Diskin, G. S., Krämer, M., Spelten, N., et al. (2020). Assessment of observational evidence for direct convective hydration of the lower stratosphere. *Journal of Geophysical Research: Atmospheres*, 125, e2020JD032793. <https://doi.org/10.1029/2020jd032793>
- Jensen, E. J., & Pfister, L. (2004). Transport and freeze-drying in the tropical tropopause layer. *Journal of Geophysical Research*, 109, D02207. <https://doi.org/10.1029/2003jd004022>

- Jensen, E. J., Thornberry, T. D., Rollins, A. W., Ueyama, R., Pfister, L., Bui, T., et al. (2017). Physical processes controlling the spatial distributions of relative humidity in the tropical tropopause layer over the Pacific. *Journal of Geophysical Research: Atmospheres*, *122*, 6094–6107. <https://doi.org/10.1002/2017jd026632>
- Kabllick, G. P., III, Allen, D. R., Fromm, M. D., & Nedoluha, G. E. (2020). Australian pyroCb smoke generates synoptic-scale stratospheric anticyclones. *Geophysical Research Letters*, *47*, e2020GL088101. <https://doi.org/10.1029/2020gl088101>
- Kahn, B. H., Gettelman, A., Fetzer, E. J., Eldering, A., & Liang, C. K. (2009). Cloudy and clear-sky relative humidity in the upper troposphere observed by the A-train. *Journal of Geophysical Research*, *114*, D00H02. <https://doi.org/10.1029/2009jd011738>
- Khaykin, S., Legras, B., Bucci, S., et al. (2020). The 2019/20 Australian wildfires generated a persistent smoke-charged vortex rising up to 35 km altitude. *Communications Earth and Environment*, *1*, 22. <https://doi.org/10.1038/s43247-020-00022-5>
- Kim, J., Randel, W. J., Birner, T., & Abalos, M. (2016). Spectrum of wave forcing associated with the annual cycle of upwelling at the tropical tropopause. *Journal of the Atmospheric Sciences*, *73*, 855–868. <https://doi.org/10.1175/jas-d-15-0096.1>
- Kim, J., & Son, S.-W. (2012). Tropical cold-point tropopause: Climatology, seasonal cycle, and intraseasonal variability derived from COSMIC GPS radio occultation measurements. *Journal of Climate*, *25*(15), 5343–5360. <https://doi.org/10.1175/jcli-d-11-00554.1>
- Kloss, C., Berthet, G., Sellitto, P., Ploeger, F., Taha, G., Tidiga, M., et al. (2021). Stratospheric aerosol layer perturbation caused by the 2019 Raikoke and Ulawun eruptions and their radiative forcing. *Atmospheric Chemistry and Physics*, *21*, 535–560. <https://doi.org/10.5194/acp-21-535-2021>
- Krämer, M., Rolf, C., Spelten, N., Afchine, A., Fahey, D., Jensen, E., et al. (2020). A microphysics guide to cirrus—Part 2: Climatologies of clouds and humidity from observations. *Atmospheric Chemistry and Physics*, *20*, 12569–12608. <https://doi.org/10.5194/acp-20-12569-2020>
- Lambert, A., Read, W., & Livesey, N. (2015). *MLS/Aura level 2 water vapor (H₂O) mixing ratio V004*. Greenbelt, MD: Goddard Earth Sciences Data and Information Services Center (GES DISC).
- Lambert, A., Read, W., & Livesey, N. (2020). *MLS/Aura level 2 water vapor (H₂O) mixing ratio V005*. Greenbelt, MD: Goddard Earth Sciences Data and Information Services Center (GES DISC).
- Livesey, N. J., Read, W. G., Froidevaux, L., Lambert, A., Manney, G. L., Pumphrey, H. C., et al. (2020). *Version 4.2x Level 2 and 3 data quality and description document* (Tech. Rep. JPL D-33509 Rev. E): Jet Propulsion Lab.
- Lorelei, S. S., Bradley, O. H., Jr., Mauldin, L. E., III, Wusk, M. B., Chu, W. P., Farwell, L. C., II, & Galeone, P. (1999). *Stratospheric aerosol and gas experiment III (SAGE III) mission aboard the International Space Station*. Proceedings of SPIE 3756, Optical Spectroscopic Techniques and Instrumentation for Atmospheric and Space Research III. <https://doi.org/10.1117/12.366370>
- Lossow, S., Khosrawi, F., Nedoluha, G. E., Azam, F., Bramstedt, K., Burrows, J. P., et al. (2017). The SPARC water vapour assessment II: Comparison of annual, semi-annual and quasi-biennial variations in stratospheric and lower mesospheric water vapour observed from satellites. *Atmospheric Measurement Techniques*, *10*, 1111–1137. <https://doi.org/10.5194/amt-10-1111-2017>
- Manney, G. L., Daffer, W. H., Zawodny, J. M., Bernath, P. F., Hoppel, K. W., Walker, K. A., et al. (2007). Solar occultation satellite data and derived meteorological products: Sampling issues and comparisons with Aura Microwave Limb Sounder. *Journal of Geophysical Research*, *112*, D24S50. <https://doi.org/10.1029/2007jd008709>
- Manney, G. L., Heggin, M. I., Daffer, W. H., Santee, M. L., Ray, E. A., Pawson, S., et al. (2011). Jet characterization in the upper troposphere/lower stratosphere (UTLS): Applications to climatology and transport studies. *Atmospheric Chemistry and Physics*, *11*, 6115–6137. <https://doi.org/10.5194/acp-11-6115-2011>
- Millán, L. F., Livesey, N. J., Santee, M. L., Neu, J. L., Manney, G. L., & Fuller, R. A. (2016). Case studies of the impact of orbital sampling on stratospheric trend detection and derivation of tropical vertical velocities: Solar occultation vs. limb emission sounding. *Atmospheric Chemistry and Physics*, *16*, 11521–11534. <https://doi.org/10.5194/acp-16-11521-2016>
- Mote, P. W., Rosenlof, K. H., McIntyre, M. E., Carr, E. S., Gille, J. C., Holton, J. R., et al. (1996). An atmospheric tape recorder: The imprint of tropical tropopause temperatures on stratospheric water vapor. *Journal of Geophysical Research*, *101*, 3989–4006. <https://doi.org/10.1029/95jd03422>
- Murphy, D. M., & Koop, T. (2005). Review of the vapour pressures of ice and supercooled water for atmospheric applications. *Quarterly Journal of the Royal Meteorological Society*, *131*, 1539–1565. <https://doi.org/10.1256/qj.04.94>
- Nützel, M., Podglajen, A., Garny, H., & Ploeger, F. (2019). Quantification of water vapour transport from the Asian monsoon to the stratosphere. *Atmospheric Chemistry and Physics*, *19*, 8947–8966. <https://doi.org/10.5194/acp-19-8947-2019>
- Ploeger, F., Günther, G., Konopka, P., Fueglistaler, S., Müller, R., Hoppe, C., et al. (2013). Horizontal water vapor transport in the lower stratosphere from subtropics to high latitudes during boreal summer. *Journal of Geophysical Research: Atmospheres*, *118*, 8111–8127. <https://doi.org/10.1002/jgrd.50636>
- Randel, W., & Park, M. (2019). Diagnosing observed stratospheric water vapor relationships to the cold point tropical tropopause. *Journal of Geophysical Research: Atmospheres*, *124*, 7018–7033. <https://doi.org/10.1029/2019JD030648>
- Randel, W. J., Moyer, E., Park, M., Jensen, E., Bernath, P., Walker, K., & Boone, C. (2012). Global variations of HDO and HDO/H₂O ratios in the upper troposphere and lower stratosphere derived from ACE-FTS satellite measurements. *Journal of Geophysical Research*, *117*, D06303. <https://doi.org/10.1029/2011jd016632>
- Randel, W. J., Zhang, K., & Fu, R. (2015). What controls stratospheric water vapor in the NH summer monsoon regions? *Journal of Geophysical Research: Atmospheres*, *120*, 7988–8001. <https://doi.org/10.1002/2015jd023622>
- Rong, P., Russell, J. M., III, Marshall, B. T., Gordley, L. L., Mlynyczak, M. G., & Walker, K. A. (2019). Validation of water vapor measured by SABER on the TIMED satellite. *Journal of Atmospheric and Solar-Terrestrial Physics*, *194*, 105099. <https://doi.org/10.1016/j.jastp.2019.105099>
- Russell, J. M., III, Gordley, L. L., Park, J. H., Drayson, S. R., Hesketh, W. D., Cicerone, R. J., et al. (1993). The halogen occultation experiment. *Journal of Geophysical Research*, *98*, 10777–10797. <https://doi.org/10.1029/93jd00799>
- Schoeberl, M. R., Jensen, E. J., Pfister, L., Ueyama, R., Wang, T., Selkirk, H., et al. (2019). Water vapor, clouds, and saturation in the tropical tropopause layer. *Journal of Geophysical Research: Atmospheres*, *124*, 3984–4003. <https://doi.org/10.1029/2018jd029849>
- Schwartz, M. J., Read, W. G., Santee, M. L., Livesey, N. J., Froidevaux, L., Lambert, A., & Manney, G. L. (2013). Convectively injected water vapor in the North American summer lowermost stratosphere. *Geophysical Research Letters*, *40*, 2316–2321. <https://doi.org/10.1002/grl.50421>
- Smith, J. B., Wilmoth, D. M., Bedka, K. M., Bowman, K. P., Homeyer, C. R., Dykema, J. A., et al. (2017). A case study of convectively sourced water vapor observed in the overworld stratosphere over the United States. *Journal of Geophysical Research: Atmospheres*, *122*, 9529–9554. <https://doi.org/10.1002/2017jd026831>
- Thomason, L. W., Burton, S. P., Iyer, N., Zawodny, J. M., & Anderson, J. (2004). A revised water vapor product for the Stratospheric Aerosol and Gas Experiment (SAGE) II version 6.2 data set. *Journal of Geophysical Research*, *109*, D06312. <https://doi.org/10.1029/2003jd004465>

- Thomason, L. W., Moore, J. R., Pitts, M. C., Zawodny, J. M., & Chiou, E. W. (2010). An evaluation of the SAGE III version 4 aerosol extinction coefficient and water vapor data products. *Atmospheric Chemistry and Physics*, *10*, 2159–2173. <https://doi.org/10.5194/acp-10-2159-2010>
- Ueyama, R., Jensen, E. J., & Pfister, L. (2018). Convective influence on the humidity and clouds in the tropical tropopause layer during boreal summer. *Journal of Geophysical Research: Atmospheres*, *123*, 7576–7593. <https://doi.org/10.1029/2018JD028674>
- Ueyama, R., Jensen, E. J., Pfister, L., & Kim, J.-E. (2015). Dynamical, convective, and microphysical control on wintertime distributions of water vapor and clouds in the tropical tropopause layer. *Journal of Geophysical Research: Atmospheres*, *120*(10), 483–10500. <https://doi.org/10.1002/2015jd023318>
- Wang, H. J. R., Damadeo, R., Flittner, D., Kramarova, N., Taha, G., Davis, S., et al. (2020). Validation of SAGE III/ISS solar occultation ozone products with correlative satellite and ground based measurements. *Journal of Geophysical Research: Atmospheres*, *125*, e2020JD032430. <https://doi.org/10.1029/2020jd032430>
- Waters, J. W., Froidevaux, L., Harwood, R. S., Jarnot, R. F., Pickett, H. M., Read, W. G., et al. (2006). The Earth Observing System Microwave Limb Sounder (EOS MLS) on the Aura satellite. *IEEE Transactions on Geoscience and Remote Sensing*, *44*(5), 1075–1092. <https://doi.org/10.1109/tgrs.2006.873771>
- World Meteorological Organization (WMO). (1957). Definition of the tropopause. *World Meteorological Organization Bulletin*, *6*, 136.
- Wright, J. S., Fu, R., Fueglistaler, S., Liu, Y. S., & Zhang, Y. (2011). The influence of summertime convection over Southeast Asia on water vapor in the tropical stratosphere. *Journal of Geophysical Research*, *116*, D12302. <https://doi.org/10.1029/2010jd015416>
- Yu, W., Dessler, A. E., Park, M., & Jensen, E. J. (2020). Influence of convection on stratospheric water vapor in the North American Monsoon region. *Atmospheric Chemistry and Physics*, *20*, 12153–12161. <https://doi.org/10.5194/acp-20-12153-2020>
- Yue, J., Russell, J., Gan, Q., Wang, T., Rong, P., Garcia, R., & Mlynchzak, M. (2019). Increasing water vapor in the stratosphere and mesosphere after 2002. *Geophysical Research Letters*, *46*, 13452–13460. <https://doi.org/10.1029/2019gl084973>